

Position and Temperature Dependence of Pyroelectricity in Domain-Engineered Stoichiometric and Congruent LiTaO₃*

JOHN H. LEHMAN and CHRIS N. PANNELL[†]

*National Institute of Standards and Technology, 325 Broadway, Boulder,
Colorado 80305-3328, USA*

[†]*School of Physical Sciences, The University of Kent, Canterbury, Kent, CT2 7NR, UK*

(Received March 15, 2003)

Domain-engineered bicell (parallel compensated) pyroelectric detectors were constructed from stoichiometric and congruent lithium tantalate. The variation of the pyroelectric current response of these detectors was investigated as a function of temperature and position. We define a pyroelectric response gradient Π , which, near boundary of antiparallel domains, is asymmetric and increases to 4% K⁻¹ in the poled half of the congruent LiTaO₃ bicell. The Π variation in the stoichiometric LiTaO₃ bicell was also asymmetric and varied only 1% K⁻¹. The contribution of the primary, secondary, and tertiary pyroelectric effects are discussed along with a summary of the stress and strain in the heated detector disk.

Keywords: Congruent, stoichiometric; lithium tantalate; lithium niobate; temperature; strain, pyroelectricity; tertiary pyroelectricity

AIP Classification: 77.70.+a, 77.84.Dy, 77.84.-s, 06.20.-f, 07.57.kp

INTRODUCTION

Among the fundamental scientific issues regarding characterization and domain studies in LiNbO₃ and LiTaO₃ is the question of material properties near the domain wall of domain-reversed plates [1]. We have investigated the pyroelectric behavior of domain-engineered congruent LiTaO₃ (CLT) and stoichiometric LiTaO₃ (SLT) over a range of temperatures near room

*Contribution of the National Institute of Standards and Technology, not subject to Copyright.

temperature and found that pyroelectric detector responsivity varies as a function of position relative to the domain wall for z -cut plates. The material which shows the most temperature and position-dependent pyroelectric response is congruent material that has been domain reversed by electric field poling. The pyroelectric response of SLT as a function of temperature and position is less temperature dependent near the domain wall and may be correlated with evidence of strain near the domain boundary [2].

Since the earliest domain-engineered (parallel compensated) pyroelectric detector, it has been claimed that such detectors have responsivity with reduced temperature dependence [3]. We have previously investigated temperature dependence of the pyroelectric response of domain-engineered pyroelectric detectors and obtained sets of results which both contradict and confirm this generalization according to the experimental conditions. In this paper we provide further evidence that supports the validity of these results, which may appear otherwise contradictory [4, 5]. Also, we update previous arguments which attempt to explain the temperature-dependent phenomena and discuss the primary, secondary, and tertiary pyroelectric contributions.

Our motivation for this investigation is to build and evaluate large-area pyroelectric detectors for laser and optical power metrology [5]. For this application it is important to quantify the variation of the detector responsivity as a function of temperature and to reduce it if possible. Temperature-dependent variation can be a significant contribution to the measurement uncertainty when using pyroelectric detectors as transfer standards for optical power metrology. Our measurements indicate that domain engineering can change the temperature dependence, but not necessarily reduce the magnitude of the pyroelectric coefficient. Furthermore, the temperature dependence is position dependent relative to the boundary of antiparallel domains.

We have evaluated SLT as well as CLT not only for the benefit of greater understanding, but also because the construction of domain-engineered (parallel compensated) CLT-based detectors we have built in the past may be replaced by SLT-based detectors in the future. Stoichiometric material differs from congruent material by virtue of its OH^{-1} concentrations and point defects [6]. The off-congruent, lithium rich ($\text{LiO}_2 \sim 58$ mol%) melt for stoichiometric processing results in lower OH^{-1} concentrations, which are possibly responsible for internal electric fields [2]. The immediate benefit of using SLT in lieu of CLT is the coercive field necessary for electric field poling is 10 times lower for SLT than for CLT (21 kV/mm for CLT compared to 1.7 kV/mm for SLT) [2]. Therefore, SLT-based domain-engineered pyroelectric detectors are potentially less expensive to build.

BACKGROUND

The expression for the pyroelectric effect consists of two terms. The first term represents what is known as *true pyroelectricity* and is sometimes referred to as the primary pyroelectric coefficient, while the second term represents what is known as *false pyroelectricity of the first kind* and may be referred to as the secondary pyroelectric coefficient. In this document the two terms are simply referred to as the first and second pyroelectric coefficients for the primary and secondary pyroelectric effects, respectively. There is also a third phenomenon, not usually expressed in a general way mathematically, known as tertiary pyroelectricity. This phenomenon is observed when measuring the pyroelectric coefficient over a range of temperatures. This tertiary pyroelectric effect is difficult to quantify and arguably is not a fundamental material property, but rather appears to be a consequence of the experimental procedure or the physical surroundings of the material being evaluated [7].

It can be difficult to measure the total pyroelectric coefficient and even more difficult to independently measure the primary and secondary coefficients near room temperature. Measurements of the pyroelectric coefficient as a function of temperature for various materials [8], from cryogenic temperatures up to the Curie temperature, indicate that the pyroelectric coefficient does not necessarily change monotonically. Furthermore, the first coefficient may decrease while the second coefficient increases over the same temperature range. As a result, for certain materials, there exists a temperature where the pyroelectric coefficient is negligible because the first and second coefficients are equal and opposite [9].

THE PYROELECTRIC RESPONSE GRADIENT

The pyroelectric current response as a function of position and temperature is given by

$$i(x, \theta) = \gamma \frac{p(x, \theta)A}{c_v h} \Phi e^{j\omega t} \quad (1)$$

where θ is the temperature of the detector plate, c_v is the specific heat of the detector material, h is the detector thickness, x defines a location some distance from the domain wall on the detector surface heated by a modulated input irradiance $\Phi e^{j\omega t}$ (small $\Delta\theta$) over an area A . The relative current response γ for a freestanding detector plate is that given by Holeman [10], Peterson *et al.* [11], Phelan and Cook [12], and Bauer and Ploss [13].

For this investigation, we define $p(x, \theta)$ as an approximation to p_3^T , which defines the variation of the pyroelectric effect as a function of position and temperature. For this discussion we are interested only in the pyroelectric gradient transverse to the domain wall. Thus, using Eq. (1), we define Π as the normalized temperature dependence of the pyroelectric coefficient, where

$$\Pi = \left[\frac{1}{\theta_{hi} - \theta_{lo}} \right] \frac{|i(x, \theta_{hi})| - |i(x, \theta_{lo})|}{|i(x, \theta_{hi})|}. \quad (2)$$

Here we assume that the temperature dependence varies linearly over a modest temperature range ($\theta = \pm 10^\circ\text{C}$) near room temperature ($\theta_{lo} = 15^\circ\text{C}$, $\theta_{hi} = 35^\circ\text{C}$). This assumption is based on temperature dependence of several different detectors evaluated in the present investigation [5].

EXPERIMENTAL SETUP

The experiments undertaken required building two domain-engineered detectors, one from CLT and the other from SLT [14, 15]. The detectors were mounted and packaged so that the crystals were stress free (no mechanical constraint for expansion and contraction) as shown in Fig. 1.

The domain-engineered plates were fabricated from z-cut 15 mm diameter, $150\ \mu\text{m}$ thick LiTaO_3 wafers by a process similar to that described by Lehman and Aust [16]. A pair of 25 nm thick Ni poling electrodes, defined by a shadow mask, was deposited onto a plate and the spontaneous polarization of those regions was reversed by applying a coercive field by means of a technique described by Meyers *et al.* [17].

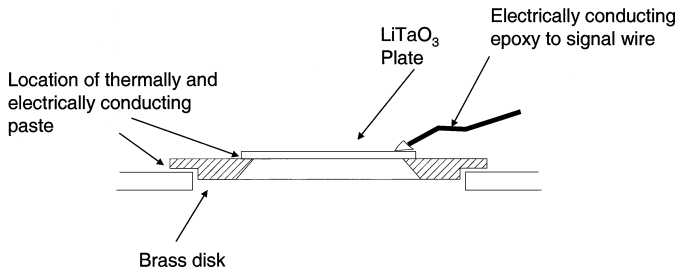


Figure 1. Schematic cross-section view of the unrestrained pyroelectric detector plate.

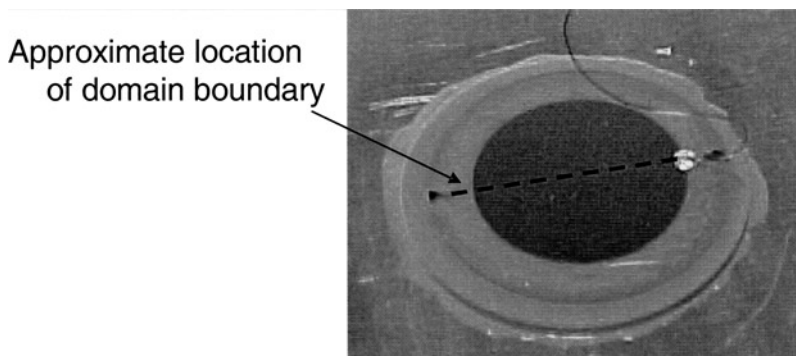


Figure 2. Photograph of the back of the unrestrained detector mounting. The dashed line indicates the approximate location of the domain boundary. (See Color Plate I)

The two domain-engineered detectors (or bicells) were then fabricated by depositing 25 nm thick Ni circular electrodes 1 cm in diameter, centered on the circular plate. These electrodes also served as a thermal absorber. A schematic cross-sectional view of the detector packaging is shown in Fig. 1 and a photograph of the construction (back facing camera) is shown in Fig. 2.

The packaged detectors were then mounted on a temperature-controlled stage. The temperature was varied and recorded by computer control. The detector responsivity was sampled and recorded from a lock-in detection scheme, shown in Fig. 3. The position of the domain wall, orientation of the crystal domains, and the translation of the probe beam (not to scale) in the $\pm x$ direction is shown in Fig. 4.

RESULTS AND DISCUSSION

The results are presented in two parts: (a) comparison of the pyroelectric response in each half of CLT and SLT bicells; (b) detailed examination of the response gradient of each bicell near the domain boundary.

(a) The Pyroelectric Response

The measured current responsivity was $0.26 \mu\text{A}/\text{W}$. The absolute responsivity of the detectors based on congruent material was the same as the stoichiometric material within $\pm 2\%$ at 20°C . The responsivity of each half of each bicell was within $\pm 1\%$ of the other. We have not thoroughly evaluated the uncertainty of this measurement because we are primarily interested in

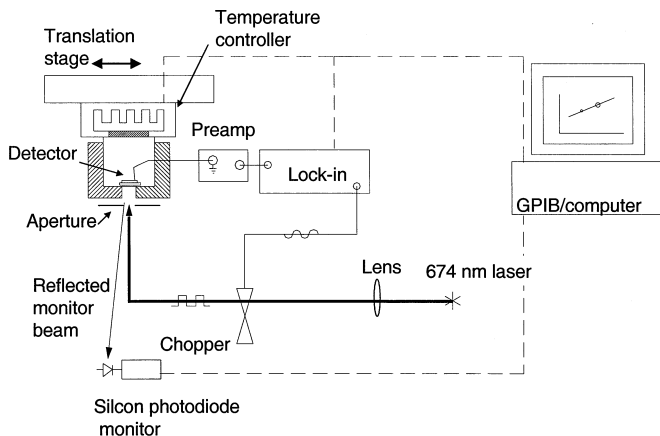


Figure 3. Schematic view of the experimental setup for the temperature dependence measurements.

the relative responsivity as a function of temperature and position of the 4 detector areas (2 devices, each having areas of equal and opposite spontaneous polarization).

The temperature dependence between 15°C and 35°C of the two domain-engineered bicell pyroelectric detectors has a positive slope when illuminated with a broadband lamp source (3400 K) covering a relatively large fraction of the detector area. The temperature dependence (slope) we measure is

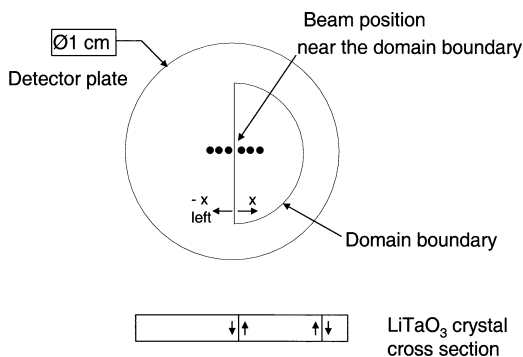


Figure 4. Representation of the relationship of the 674 nm wavelength probe beam and the domain-engineering boundary. Beam size less than 0.2 mm diameter (that is, 99% of power within a 0.2 mm diameter).

0.75% K⁻¹. The temperature dependence has been reported for congruent LiTaO₃ and LiNbO₃ to be anywhere between 4% K⁻¹ to 0.1% K⁻¹ with various mounting conditions [4, 18].

(b) Response Gradient Near the Domain Boundary

The temperature dependence of the detector response near the domain boundary was examined in greater detail. In principle, the measurement is identical to (a), with the additional procedure of probing the detector response at incremental positions (10 μm increments) with a 0.2 mm diameter, 674 nm wavelength laser along a line perpendicular to the domain wall. The measurement of temperature dependence as a function of position was repeated at 15°C and 35°C. The measurement result, on the basis of position for both 15°C and 35°C are shown in Fig. 5. The data $R(x, \theta)$ are expressed as the ratio of the current response $i(x, \theta)$ to the response $i(200, \theta)$ far from the domain wall (that is, $x = 200 \mu\text{m}$). The ratio of the response at each position and at the two temperature extremes were calculated as shown in Eq. (2). The result of this calculation is shown in Fig. 6. The procedure was repeated with the SLT bicell. The results of this measurement are shown along with those from the CLT bicell in Fig. 7.

The relative response in Fig. 5 is proportional to the pyroelectric coefficient in Eq.(1). The total pyroelectric coefficient (constant

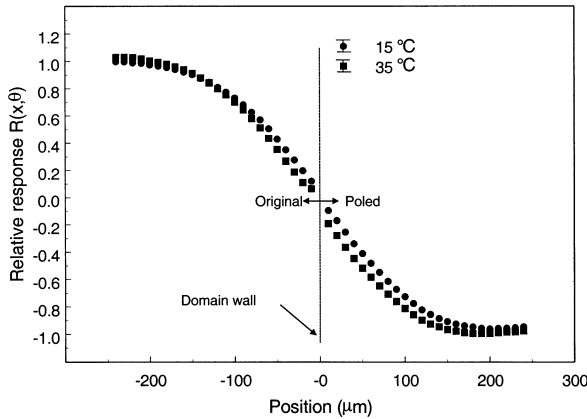


Figure 5. Relative current response of the CLT bicell near the domain boundary evaluated at a detector temperature of 15°C (●) and 35°C (■).

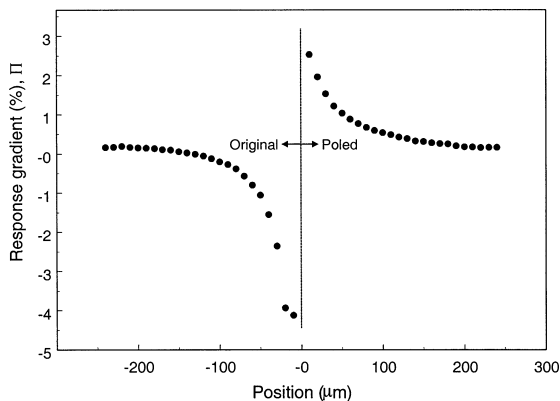


Figure 6. Response gradient calculated using the data from Fig. 6 using Eq. (2).

stress) [7] is

$$p_3^T = p_3^S + [2\alpha_1(d_{31}^T c_{11} + d_{31}^T c_{12} + d_{33}^T c_{13}) + \alpha_3(2d_{31}^T c_{13} + d_{33}^T c_{33})], \quad (3)$$

where α_1 are the coefficients of thermal expansion, d_{ij} are the piezoelectric strain coefficients, and c_{ij} are the elastic stiffness coefficients (note: the subscript notation in capital letters indicates matrix notation, while the small letters are tensor notation [19]). For LiTaO_3 , $p_3^T = 19 \text{ nC cm}^{-2} \text{ K}^{-1}$ [20]. The secondary pyroelectric coefficient for LiTaO_3 is the bracketed portion

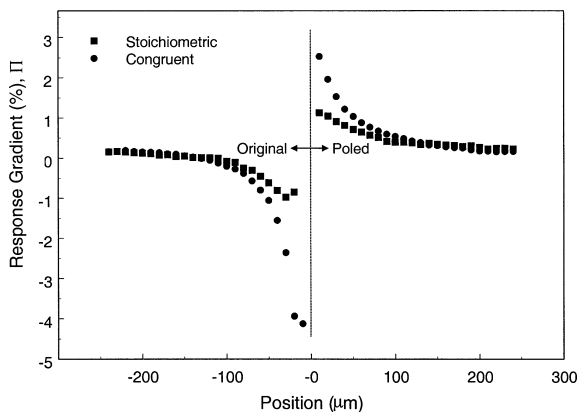


Figure 7. Response gradient of CLT bicell compared with SLT bicell.

of Eq. (3), which is

$$p_{3\text{secondary}} = [2\alpha_1(d_{31}^T c_{11} + d_{31}^T c_{12} + d_{33}^T c_{13}) + \alpha_3(2d_{31}^T c_{13} + d_{33}^T c_{33})]. \quad (4)$$

Therefore, the calculated value of the secondary pyroelectric coefficient (using values given by Smith and Welsh [21]) is $-0.7 \text{ nC cm}^{-2} \text{ K}^{-1}$. The value of the pyroelectric coefficient is noteworthy for three reasons: (1) The magnitude of the secondary coefficient is less than 4% of the total pyroelectric coefficient; (2) the secondary coefficient is negative while the total coefficient is positive; (3) the total coefficient is uniform as a function of position if we assume that the material properties are also uniform.

Our experimental results might indicate that either the primary or secondary pyroelectric effect is being suppressed (or favored) near the domain wall, and that the gradient we observe is proportional to the change in either coefficient. However we must also consider the relationship of stress, strain, and temperature of the detector disk. We know from Gopalan *et al.* [6], that there is residual strain near the domain boundary of antiparallel domains and that the strain is lower for SLT than for CLT. We have confirmed this by observing the change in index of refraction at the domain boundary of the CLT and SLT samples. We know from Nye [7] that tertiary pyroelectricity is the result of a “nonuniform state of affairs.” According to Nye’s explanation, the non-uniform state is the result of temperature gradients, which are responsible for non-uniform stresses and strains. In this case, we assert that the temperature gradients are negligible, but that non-uniform strain exists because of antiparallel domains, and this strain modifies the pyroelectric response as a function of position near the domain boundary. The question remains whether the gradients we observe may be attributed to tertiary pyroelectricity and if so, whether it can be quantified.

The appendix summarizes the thermally induced stress in a thin disk for uniform or partial heating, for either a clamped or freely suspended disk. Our experimental design matches the case of partial heating of a clamped disk. As indicated in the appendix, whether the detector disk is clamped or freely suspended is irrelevant if we heat only a small portion of the disk, far from the disk perimeter. From this, we expect the response gradient to be zero and the pyroelectric coefficient to be constant as a function of position. Our results indicate that this is not the case. The absolute value of Π is greater than three near the domain wall of the CLT bicell. The gradient increases as the area of heating nears the domain boundary. The gradient is relatively smaller for the SLT bicell. Therefore, it is more plausible that the response

gradient is the result of tertiary pyroelectricity, which is a result of a strain gradient near the domain wall, rather than variation of the first or second pyroelectric coefficients.

CONCLUSION

We found that the temperature dependence of the pyroelectric response of both CLT and SLT is not constant when probed with a laser light source covering a relatively small fraction of the detector area. However, the variation may be correlated with the position of the probe beam relative to the boundary of antiparallel domains. The slope of the temperature dependence (the pyroelectric response gradient, Π) of the pyroelectric coefficient varies relative to the position of a domain boundary. The gradient is larger for CLT, than it is for SLT. In the absence of domain boundaries, the state of stress and strain in a heated pyroelectric detector depends on the mechanical boundary conditions and the size of the area of heating. Equations in the appendix treat three cases: (1) uniform heating of an entire clamped detector disk; (2) uniform heating of an entire unclamped detector disk; (3) heating of a small area away from the edge of a clamped or unclamped detector disk. The heating and clamping of the detectors we have investigated are best represented by the third case, but it does not account for the gradient we observe. We attribute the pyroelectric response gradient to the tertiary pyroelectric effect, which is the result of strain near the domain boundary.

REFERENCES

- [1] V. Gopalan, N. Sanford, J. A. Aust, K. Kitamura, and Y. Furukawa, "Crystal growth characterization, and domain studies in lithium niobate and lithium tantalate ferroelectrics," *Handbook of Advanced Electronic and Photonic Materials and Devices* Vol. 4, edited by H.S. Nalwa, 57–114 (2001).
- [2] K. Kitamura, Y. Furukawa, K. Niwa, V. Gopalan, and T. Mitchell, "Crystal growth and low coercive field 180° domain switching characteristics of stoichiometric LiTaO₃," *Appl. Phys. Lett.* **73**, 3073–3075 (1998).
- [3] N. E. Byer, S. E. Stokowski, and J. D. Venables, "Complementary domain pyroelectric detectors with reduced sensitivity to mechanical vibrations and temperature changes," *Appl. Phys. Lett.* **27**, 639–641 (1975).
- [4] J. H. Lehman, A. M. Radojevic, and R. M. Osgood Jr., "Domain-engineered thin-film LiNbO₃ pyroelectric-bicell optical detector," *IEEE Phot. Tech. Lett.* **13**, 851–853 (2001).
- [5] J. Lehman, G. Eppeldauer, J. A. Aust, and M. Racz, "Domain Engineered pyroelectric radiometer," *Appl. Opt.* **38**, 7047–7055 (1999).
- [6] V. Gopalan and M. Goppta, "Origin of internal fields and visualization of 180° domains in congruent LiTaO₃ crystals," *J. Appl. Phys.* **80**, 6099–6106 (1996).

- [7] J. F. Nye, *Physical Properties of Crystals* (Clarendon Press, Oxford, 1957), pp. 189–191.
- [8] See e.g., S. B. Lang, *Sourcebook of pyroelectricity* (Gordon and Breach Science Publisher, New York, 1974), p. 20.
- [9] S. B. Lang, “Pyroelectric coefficient of lithium sulfate monohydrate,” *Phys. Rev. B* **4**, 3603 (1971).
- [10] B. R. Holeman, “Sinusoidally modulated heat flow and the pyroelectric effect,” *Infr. Phys.* **12**, 125–135 (1972).
- [11] R. L. Peterson, G. W. Day, P. M. Gruzensky, and R. J. Phelan Jr., “Analysis of Response of Pyroelectric Optical Detectors,” *J. Appl. Phys.* **45**, 3296–3303 (1974).
- [12] R. J. Phelan Jr. and A. R. Cook, “Electrically calibrated pyroelectric optical-radiation detector,” *Appl. Opt.* **12**, 2494–2500 (1973).
- [13] S. Bauer and B. Ploss, “Method for the measurement of the thermal, dielectric, and pyroelectric properties of thin pyroelectric films and their applications for integrated heat sensors,” *J. Appl. Phys.* **68**, 6361–6367 (1990).
- [14] Manufacturer Congruent LiTaO₃, MolTech, GmbH, Rudower Chaussee 29-31 (OWZ), 12489 Berlin, Germany.
- [15] Manufacturer Congruent LiTaO₃, OXIDE Corporation, 9633, Kobuchisawa, Kitakoma, Yamanashi 408-0044 Japan.
- [16] J. H. Lehman and J. A. Aust, “Bicell pyroelectric detector made from a single LiNbO₃ domain-reversed electret,” *Appl. Opt.* **37**, 4210–4212 (1998).
- [17] L. E. Meyers, R. C. Eckardt, M. M. Fejer, R. L. Byer, W. R. Bosenberg, and J. W. Pierce, “Quasi-phase-matched optical parametric oscillators in bulk periodically poled LiNbO₃,” *J. Opt. Soc. Am. B* **12**, 2102–2116 (1995).
- [18] N. E. Byer, S. E. Stokowski, and J. D. Venables, “Complementary domain pyroelectric detectors with reduced sensitivity to mechanical vibrations and temperature changes,” *Appl. Phys. Lett.* **27**, 639–641 (1975).
- [19] J. F. Nye, *Physical Properties of Crystals* (Clarendon Press, Oxford, 1957), pp. 134–135.
- [20] M. E. Lines and A. M. Glass, “Primary pyroelectric effect in LiTaO₃,” *Phys. Rev. Lett.* **39**, 1362–1364 (1977).
- [21] R. T. Smith and F. S. Welsh, “Temperature dependence of the elastic, piezoelectric, and dielectric constants of lithium tantalate and lithium niobate,” *J. Appl. Phys.* **42**, 2219–2230 (1971).
- [22] S. P. Timoshenko and J. N. Goodier, *Theory of Elasticity* (McGraw Hill, New York, 1970), p. 66.
- [23] L. B. Schein, P. J. Cressman, and L. E. Cross, “Electrostatic measurements of unusually large secondary pyroelectricity in partially clamped LiNbO₃,” *Ferroelectrics* **22**, 937–943 (1979).
- [24] H. Gnewuch, N. K. Zayer, C. N. Pannell, G. W. Ross, and P. G. R. Smith, “Broadband monolithic acousto-optic tunable filter,” *Opt. Lett.* **25**, 305–307 (2000).

APPENDIX: STRESS, STRAIN, AND THE PYROELECTRIC COEFFICIENT FOR LiTaO₃ AND LiNbO₃

The behavior of the pyroelectric coefficient for a z-cut pyroelectric plate depends on properties of the crystal from which the plate is made, the geometry and physical mounting of the plate, and the volume of heating.

We limit the present discussion to LiTaO_3 and LiNbO_3 and consider the mathematical implications of a circular plate that is clamped around the perimeter, partially clamped, or simply supported (entirely unconstrained). A complete discussion is lengthy because the mathematics of the derivation includes manipulation of third- and fourth-order tensors. However a complete description of the pyroelectric coefficient is important and we summarize the description by way of stating the essential points. We abbreviate the discussion by considering the materials to have an isotropic modulus elasticity E and a coefficient of thermal expansion α based on an average of the direction-dependent values (the digression from the full 3 m crystal properties to the isotropic approximation is not given).

The equation of equilibrium for a plate in cylindrical-polar coordinates (r, ϕ) is given by Timoshenko and Goodier [22] in the form of

$$\frac{\partial \sigma_{rr}}{\partial r} + \frac{1}{r} \frac{\partial \sigma_{r\phi}}{\partial \phi} + \frac{\sigma_{rr} - \sigma_{\phi\phi}}{r} + R = 0 \quad (5)$$

and

$$\frac{\partial \sigma_{\phi\phi}}{\partial \phi} + \frac{1}{r} \frac{\partial \sigma_{r\phi}}{\partial r} + \frac{2\sigma_{r\phi}}{r} + S = 0 \quad (6)$$

where R is the body force density [N m^{-3}] in the \hat{r} direction and S is the body force density in the $\hat{\phi}$ direction. The notation for stress and strain based on the symbols σ and ϵ with subscripts r , ϕ , and z is used to distinguish the stress and strain tensors in cylindrical polar coordinates. The components of the stress tensor have the conventional form

$$T_{jk} = \begin{bmatrix} \sigma_{rr} & \sigma_{r\phi} & \sigma_{rz} \\ \sigma_{\phi r} & \sigma_{\phi\phi} & \sigma_{\phi z} \\ \sigma_{zr} & \sigma_{z\phi} & \sigma_{zz} \end{bmatrix}. \quad (7)$$

A plate section relative to the coordinate system is shown in Fig. 8.

We assume that the temperature of the plate does not vary over the thickness; hence, the stress and strain also do not vary in the z direction and $\sigma_{rz} = \sigma_{\phi z} = \sigma_{zz} \equiv 0$ we define as a boundary condition. Thus Eqs. (5) and (6) reduce to

$$\frac{\partial \sigma_{rr}}{\partial r} + \frac{\sigma_{rr} - \sigma_{\phi\phi}}{r} = 0 \quad (8)$$

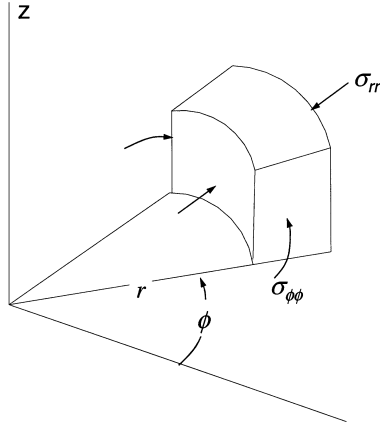


Figure 8. Coordinate system relative to a plate section with stresses σ_{rr} and $\sigma_{\phi\phi}$.

and because we assume axial symmetry of heating at the center of the plate

$$\sigma_{r\phi} = 0. \quad (9)$$

Given the development so far, for plane stress, Hooke's law takes the form in plane-polar coordinates

$$\begin{aligned} \epsilon_{rr} &= \frac{1}{E}(\sigma_{rr} - \nu\sigma_{\phi\phi}) \\ \epsilon_{\phi\phi} &= \frac{1}{E}(\sigma_{\phi\phi} - \nu\sigma_{rr}) \\ \epsilon_{r\phi} &= \frac{1+\nu}{E}(\sigma_{r\phi}). \end{aligned} \quad (10)$$

Timoshenko and Goodier [22] indicate that the typical stress-strain relationships are modified for thermal expansion, because some of the strain is due to thermal expansion and some is due to stress: thus if ϵ_{rr} represents the actual radial strain, $(\epsilon_{rr} - \alpha\theta)$ represents the part due to stress and Hooke's law. In this case the stress-strain relationship is correctly expressed as

$$\epsilon_{rr} - \alpha\theta = \frac{1}{E}(\sigma_{rr} - \nu\sigma_{\phi\phi}) \quad (11)$$

and

$$\epsilon_{\phi\phi} - \alpha\theta = \frac{1}{E}(\sigma_{\phi\phi} - \nu\sigma_{rr}). \quad (12)$$

Thus

$$\sigma_{rr} = \frac{E}{1 - \nu^2} [\epsilon_{rr} + \nu\epsilon_{\phi\phi} - (1 + \nu)\alpha\theta] \quad (13)$$

and

$$\sigma_{\phi\phi} = \frac{E}{1 - \nu^2} [\epsilon_{\phi\phi} + \nu\epsilon_{rr} - (1 + \nu)\alpha\theta]. \quad (14)$$

When Eqs. (13) and (14) are substituted into Eq. (8) the equilibrium equation now has the form

$$r \frac{d}{dr} (\epsilon_{rr} + \nu\epsilon_{\phi\phi}) + (1 - \nu)(\epsilon_{rr} - \epsilon_{\phi\phi}) = (1 + \nu)\alpha r \frac{d\theta}{dr}. \quad (15)$$

If u denotes the radial displacement field, then

$$\begin{aligned} \epsilon_{rr} &= \frac{du}{dr} \\ \epsilon_{\phi\phi} &= \frac{u}{r}. \end{aligned} \quad (16)$$

Substituting Eqs. (16) into Eq. (15) yields for the radial displacement

$$\frac{d^2u}{dr^2} + \frac{1}{r} \frac{du}{dr} + \frac{u}{r^2} = (1 + \nu)\alpha r \frac{d\theta}{dr}. \quad (17)$$

Integrating Eq. (17), we find

$$u = \frac{(1 + \nu)\alpha}{r} \int_0^r \theta(r) r dr + \left[C_1 r + \frac{C_2}{r^2} \right] \quad (18)$$

where the lower limit of integration is arbitrary and we choose $r = 0$ for the center of the disk coincident with the circular area of heating. The stresses can now be found using Eqs. (18) substituted into Eq. (16) and then into Eqs. (13) and (14). Timoshenko and Goodier [22] state this as

$$\sigma_{rr} = -\frac{\alpha E}{r^2} \int_0^r \theta(r) r dr + \frac{E}{1 - \nu^2} \left[C_1(1 + \nu) - C_2 \frac{(1 - \nu)}{r^2} \right] \quad (19)$$

and

$$\sigma_{\phi\phi} = \frac{\alpha E}{r^2} \int_0^r \theta(r) r dr - \alpha E \theta + \frac{E}{1 - \nu^2} \left[C_1(1 + \nu) - C_2 \frac{(1 - \nu)}{r^2} \right] \quad (20)$$

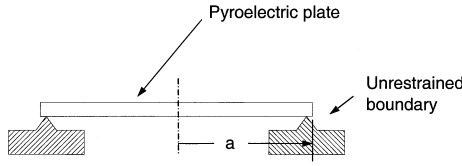


Figure 9. A pyroelectric plate unconstrained (no clamping, resting on a surface).

where C_1 and C_2 are determined from the boundary conditions.

For an unrestrained disk shown in Fig. 9 of radius a , $C_2 = 0$, and

$$C_1 = (1 - \nu) \frac{\alpha}{a^2} \int_0^a \theta(r) r dr. \quad (21)$$

Therefore Eqs. (19) and (20) become

$$\sigma_{rr} = \alpha E \left\{ \frac{1}{a^2} \int_0^a \theta(r) r dr - \frac{1}{r^2} \int_0^r \theta(r) r dr \right\} \quad (22)$$

and

$$\sigma_{\phi\phi} = \alpha E \left\{ \frac{1}{a^2} \int_0^a \theta(r) r dr + \frac{1}{r^2} \int_0^r \theta(r) r dr - \theta(r) \right\}. \quad (23)$$

For a disk clamped around its perimeter as shown in Fig. 10, $C_2 = 0$,

$$C_1 = (1 + \nu) \frac{\alpha}{a^2} \int_0^a \theta(r) r dr - \alpha \theta(a), \quad (24)$$

and for $r = a$, Eqs. (19) and (20) become

$$\sigma_{rr} = -\alpha E \left\{ \frac{1}{a^2} \int_0^a \theta(r) r dr - \frac{E}{(1 - \nu^2)} C_1 (1 + \nu) \right\} \quad (25)$$

and

$$\sigma_{\phi\phi} = \frac{\alpha E}{a^2} \int_0^a \theta(r) r dr + \frac{E}{(1 - \nu^2)} C_1 (1 + \nu) - \alpha E \theta(a). \quad (26)$$

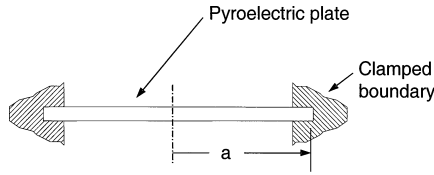


Figure 10. A pyroelectric plate clamped about its perimeter.

SUMMARY OF BOUNDARY CONDITIONS IN RELATION TO SPONTANEOUS POLARIZATION

Uniform Heating of a Thin Circular Disk

For a pyroelectric detector for which the incident optical beam area is comparable to the detector area, the mounting conditions are relevant to the temperature dependence of the responsivity. For the first approximation, we consider the plate to be mechanically isotropic, by way of using the modulus of elasticity E , Poisson's ratio ν , and coefficient of thermal expansion α .

For a *freely suspended* disk with uniform heating, $\sigma_{rr} = \sigma_{\phi\phi} = 0$, $\sigma_{zz} = 0$. For the steady state condition when the temperature of the volume of the disk heated by the optical beam, the piezoelectric contribution to the pyroelectric effect is small. At the onset of heating by the optical beam, the temperature within the crystal is nonuniform (in the z direction) and the piezoelectric contribution is varying (until the temperature reaches steady state).

For a *clamped* disk and uniform heating; $\sigma_{rr} = \sigma_{\phi\phi} = -\alpha E\theta$. Thus even after the plate temperature has reached steady state, stresses are present which will contribute to the pyroelectric coefficient with the spontaneous polarization

$$P_3 = (\sigma_{rr} + \sigma_{\phi\phi})d_{31} \quad (27)$$

The contribution is the differential

$$\frac{\partial P_3}{\partial \theta} = -2\alpha E d_{31}, \quad (28)$$

where α and E are the coefficient of thermal expansion and modulus of elasticity. If the partial derivative of Eq. (28) changes with temperature, it is because α , E , or d_{31} changes with temperature. Smith *et al.* [21] give data specifically for the temperature coefficients of α and d_{31} and the elasticity.

Heating of a Small Circular Fraction of a Thin Circular Disk

For either a freely suspended or clamped disk illuminated with a circular optical beam (not near the perimeter of the disk), much smaller than the detector diameter, is considered by Schein *et al.* [23]. The material surrounding the heated region clamps the heated region, forcing radial and tangential strains to be zero at the boundary of the heated region. That is

$$\epsilon_{rr} = \epsilon_{\phi\phi} = 0. \quad (29)$$

In this case the origin of the cylindrical-polar coordinate system is always taken at the center of the beam area. Schein *et al.* [23] give the equation

$$\sigma_{rr}(0, \theta) = \sigma_{\phi\phi}(0, \theta) = -\frac{1}{2}\alpha E\theta \quad (30)$$

so that

$$\frac{\partial P_3}{\partial \theta} = -\alpha E d_{31}. \quad (31)$$

Nonuniform Heating or Nonuniform Stress in a Thin Circular Disk

The case of nonuniform heating over the heated area, due to a nonuniform optical beam was done by Schein *et al.* [23]. Additional treatment is necessary for the case of nonuniform stress introduced by the mounting condition or the presence of a domain wall. The material variables in Eqs. (28) and (31), that is the coefficient of thermal expansion (α), Young's modulus (E), and the piezoelectric strain coefficient (d_{ij}) are spatially homogeneous and, in principle, unchanged by domain reversal (with the exception that the piezoelectric strain coefficient reverses its polarity with domain reversal [24]). Therefore, Eq. (31) is not explicitly useful for understanding the pyroelectric response gradient. The challenge remains whether the strain and hence nonuniform stress in the detector region near the boundary of antiparallel domains may be quantified and correlated with the pyroelectric response gradient.